Tribology Letters (2026) 74:39
https://doi.org/10.1007/s11249-026-02136-x

ORIGINAL PAPER

Geometry-Driven Asymmetric Tribological Response in Laser-Patterned Cu Surfaces

Sebastian Suarez[1] · Bruno Alderete[1] · Fabian Bonner[1] · Silas Schütz[1] · Frank Mücklich[1]

Received: 4 December 2025 / Accepted: 25 March 2026 / Published online: 2 April 2026

Abstract
This study investigates the fabrication of anisotropic saw-tooth topographies on copper surfaces using direct laser interference patterning (DLIP). By varying the structural periodicity (2, 7.5, and 10 µm) and manufacturing inclination angles (15, 30, and 45°), this work assesses the impact of periodic, deterministic surface topography on tribological performance. Linear reciprocating sliding tests against a hard ceramic counterbody demonstrated that these laser-patterned structures can successfully induce significant frictional anisotropy, while enduring 200 sliding cycles. A maximum frictional asymmetry coefficient of 77% was achieved for structures with a 7.5 µm periodicity manufactured at a 15° inclination angle. The results establish that maximizing asymmetry relies on generating shallower flank slopes; conversely, parameters producing steeper slopes resulted in similar friction coefficients regardless of sliding direction, minimizing the desired anisotropic effect. Regarding wear behavior, the grooves of the structured surfaces acted as effective reservoirs for worn material. Shallower manufacturing angles yielded deeper structures, which improved debris-retention capacity and maintained a mild wear regime by reducing the likelihood of three-body abrasion. The results showcase the ability to systematically tune the friction coefficient through laser-based surface modification techniques, highlighting the effects on friction and wear of deterministic asymmetrical geometries. The findings offer significant potential for applications such as sliding electrical connectors, where optimizing the ratio between insertion and retention forces is critical.

Keywords Direct laser interference patterning · Copper · Friction asymmetry

1 Introduction

In certain complex engineering applications, it becomes necessary to re-evaluate the design approach for tribological systems. Separable electrical contacts present a challenge as they require low insertion force for ease of connection and high removal force to prevent unwanted disconnection [1]. One approach to achieve this conflicting behavior is by generating frictionally asymmetrical surfaces. Friction asymmetry means that the coefficient of friction (COF) changes depending on the sliding direction. Because of a surface's specific design, sliding in one direction can have a significantly lower COF (for connection) than sliding in the opposite direction (for disconnection). Nature provides numerous examples of asymmetric friction, which are often utilized for locomotion and directional control of motion or fluid transport, such as the adhesive structures of geckos, the ventral scales of snakes, insect attachment pads, and shark skin denticles [2], and have therefore inspired the design of artificial anisotropic surfaces.

Another noteworthy natural application of frictional asymmetry is observed in wheat awns, where their oriented spikelets favor the self-planting of seeds due to a low soil penetration force [3]. In the opposite direction, these spikelets provide resistance against pull out; thus promoting the seeds' successful dispersal and germination.

Artificial interlocking structures have already been reported in the literature, showing interesting behavior particularly at the microscopic level. In a previous study by Rosenkranz and coworkers [4], Direct Laser Interference Patterning (DLIP) was chosen as the tool to generate deterministic line-like patterns on metallic surfaces. It was observed that depending on the relative orientation of the structures in both contacting bodies, it is possible to either

✉ Silas Schütz
silas.schuetz@uni-saarland.de

1 Chair of Functional Materials, Department of Materials Science and Engineering, Saarland University, 66123 Saarbrücken, Germany

minimize the contact area (lower friction) or favor mechanical interlocking (higher friction). This effect becomes more marked for lower structural periodicities.

This work explores a new approach that also deploys DLIP as a surface tailoring tool, but in this case, to generate inclined (saw-tooth) structures on a Cu surface. The obtained surfaces are subsequently tribologically characterized, and their frictional asymmetry is quantified to evaluate the configuration that presents the strongest anisotropic behavior.

2 Materials and Methods

The samples evaluated in this work were pure Cu plates (C10200 Cu-OF grade, Wieland). The surfaces (25 × 10 mm^2) were structured by DLIP on an RDX 500 Nano laser system (Pulsar Photonics) equipped with an EdgeWave INNOSLAB laser with a laser wavelength of 532 nm and a pulse duration of 12 ps.

The optical set up is presented schematically in Fig. 1. The incident laser beam strikes a diffractive optical element (DOE) parallel to the optical axis (dashed line). The DOE splits the incident beam into four diverging beams. These hit a four-sided ground glass prism in the housing of the module, which parallelizes the beams. The parallel beams now fall onto the aperture, which blocks two of the four beams to enable double-beam interference. The lens refracts each beam at an angle θ, and the incident beams come together on the sample at the overlap point. This focal point must be exactly on the sample's surface, as this is where the interference takes place. The prism can be moved to determine the path difference of the beams. Together with the lens, this influences the angle of incidence θ and thus the structural periodicity Λ, following $\Lambda = \lambda/2\bullet\sin(\theta)$, where λ is the laser's wavelength. Using this system, full-surface structures with different periodicities (i.e., 2, 7.5, and 10 µm) were produced. A rotational stage was used to tilt the sample during processing, thereby enabling the imprinting of the periodicities at different angles relative to the horizontal direction. In this work, four different inclinations were considered, 0, 15, 30, and 45°. The processing parameters used to produce the samples subject to this work are summarized in Table 1. All samples were fabricated at a scanning speed of 20 mm/s in a bidirectional movement (the laser processing parameters are found in Table S1 in the supplementary material). Further procedural details can be found in [1, 5].

The friction analysis was carried out by ball-on-flat tribometry on a CSM Nanotribometer (shown in Fig. 2a). Sliding tests were performed on the structured surfaces against an Al_2O_3 spherical counterbody (3 mm diameter, GD28 grade, HIS-Solutions) at a set load of 100 mN (F_N). The samples were tested for 200 cycles in linear reciprocating mode (with a sinusoidal trajectory), achieving a maximum linear speed of 1 mm/s. The stroke length was set to 600 µm, and the data acquisition frequency was set at 120 Hz. The temperature and humidity were kept constant for all the tests (24.5 ± 0.5 °C and 4.5 ± 0.5%, respectively). Measurements were taken perpendicularly to the line structures at three points in the center of the surface to eliminate edge effects.

To analyze the directional dependency of friction, the reciprocating sliding motion was divided into two distinct directions, as illustrated in Fig. 2b. The "DOWN" direction is defined as the forward stroke where the counterbody slides along the gentler, less steep flank of the saw-tooth structures. Conversely, the "UP" direction refers to the reverse stroke where the counterbody moves against the steeper flank of the structures. This convention is critical for understanding the intended "mechanical ratchet" effect, where motion is favored in the "DOWN" direction (lower COF) and resisted in the "UP" direction (higher COF).

The topography of the laser-structured surfaces and the morphology of the wear tracks were characterized by confocal laser scanning microscopy (CLSM) on an Olympus

Table 1 Summary of characteristics of the produced surfaces

		Inclination angle /°			
		0	15	30	45
Structural period /µm	2	✓	✓	✓	✓
	7.5	×	✓	×	×
	10	×	✓	×	×

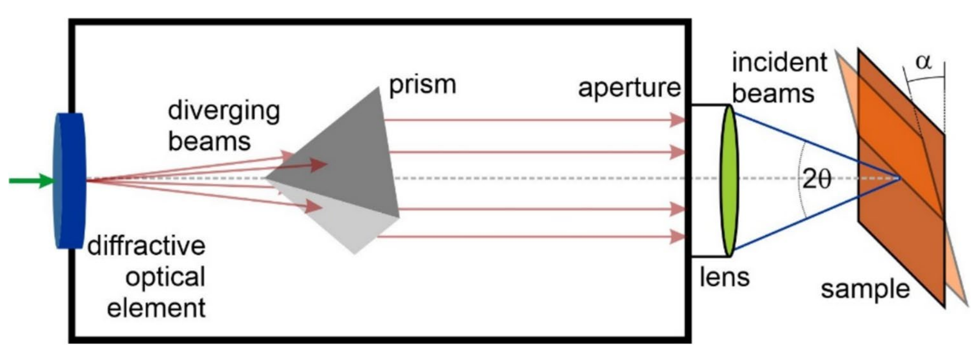

Fig. 1 Schematic setup of the optical head with an adjustable lens

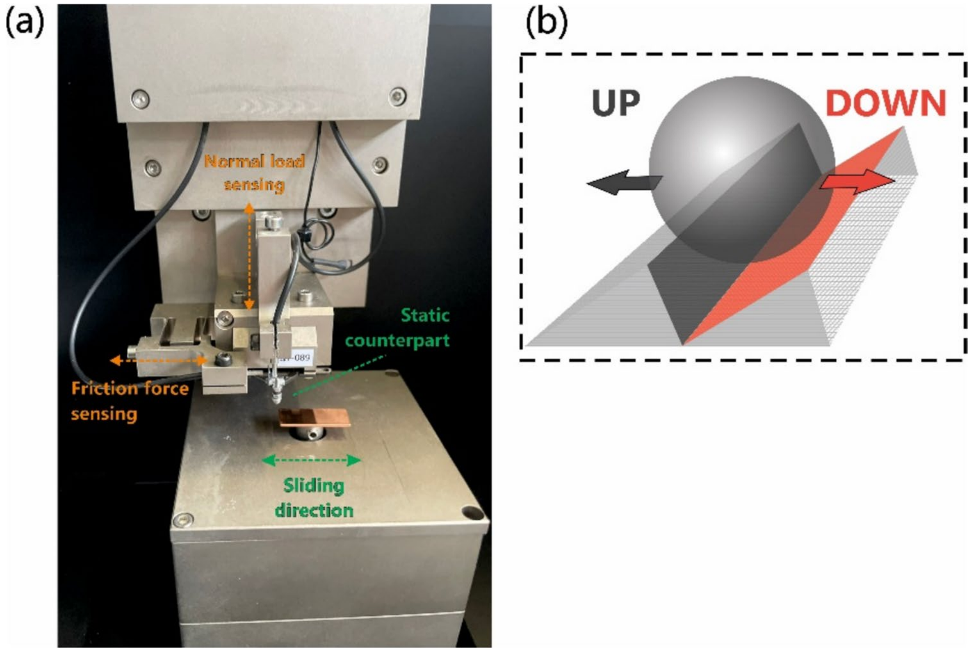

Fig. 2 **a** Schematic representation of the ball-on-flat tribometer in linear reciprocating mode. **b** Naming convention of the coefficient of friction for this study

OLS 4100 device. The device utilizes a 405 nm laser and a 50 × objective with a numerical aperture (N.A.) of 0.95. This configuration enables vertical and horizontal resolutions of 10 nm and 120 nm, respectively. Further characterization was carried out by scanning electron microscopy (SEM) on an FEI Helios NanoLab600 dual beam workstation, acquiring secondary-electron micrographs with an acceleration voltage of 5 kV. The evaluation of the wear tracks and the surrounding regions containing wear debris was performed with the aid of a trainable Weka segmentation routine [6].

3 Results and Discussion

3.1 Characterization of the Produced Structures

The optical characterization of the produced structures shows homogeneous surfaces without any recognizable resolidified material on top (Fig. 3). This is of particular significance given that the structuring process can occasionally generate irregularities due to the redeposition of evaporated material [7]. Tribologically, it might be of particular criticality if the nature of the redeposited particles is oxidic, which might negatively influence the friction and

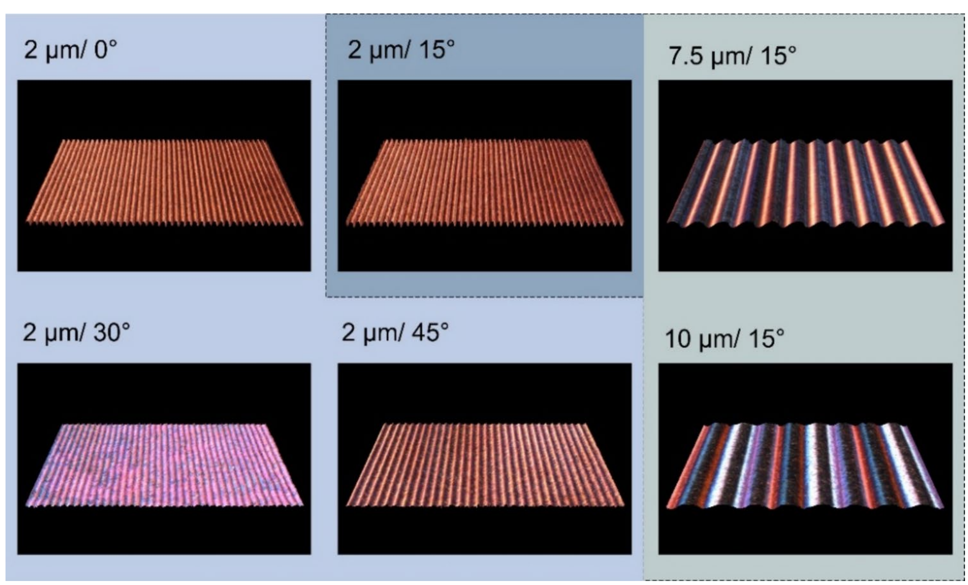

Fig. 3 Confocal laser scanning micrographs showing an overview of the produced surfaces. The field of view is (86 × 86) μm^2

wear behavior [8], as well as the electrical performance at the interface [9, 10]. Further plots of the structural profile of the produced samples are found in Figure S1 from the supplementary material.

In order to develop a better understanding of the processing of the Cu surfaces, three surface descriptors were selected as quantitative indicators of the topography. The chosen parameters are the mean height R_c, the profile skewness R_{sk}, and the profile kurtosis R_{ku} [11]. R_c is calculated for the height difference between the adjacent peaks and valleys within the evaluation length. Profile skewness is a quantitative metric used to evaluate the degree of imbalance in the height data relative to its mean line. Skewness can be interpreted as the tendency of the height points to cluster above or below the mean line. In essence, a negative R_{sk} indicates that a greater percentage of the data is located above the mean line, whereas a positive R_{sk} signifies that a higher fraction of the data lies below the mean line. R_{ku} complements the height characterization by evaluating the sharpness in the distribution. The center value for R_{ku} is 3, indicating a normal height distribution. Values below this one (i.e., *platykurtic*) indicate a surface profile characterized by a uniform distribution of heights, with minimal variation in peak height. Conversely, R_{ku} values over 3 (i.e., *leptokurtic*) indicate a surface profile characterized by numerous elevated peaks or profound troughs, suggesting that the height distribution exhibits a pronounced peak sharpness [12]. From a tribological standpoint, the descriptive parameters offer insight into the potential performance of the surface.

Table 2 summarizes the values for the produced surfaces. The structural depth R_c shows two well-defined ranges as a function of the inclination. For lower angles (0° and 15°), the values range between 1.5 and 2 µm, whereas for larger angles (30° and 45°), the depth is lower at about 0.6–0.7 µm. These substantial challenges that emerge for large inclinations are due to lower optical absorption, resulting in shallower structures while maintaining discernible saw-tooth profiles. As discussed by Alamri et al. [13], the structural depth is related to the absorption depth and the laser fluence by the Lambert–Beer law, where the depth is proportional to the logarithmic value of the cosine of the inclination angle. The S-ratio (ratio of the total surface area to the projected area) shows three ranges, where the largest ratios are observed for the lowest inclinations (for 2 µm). This does not hold for larger periodicities (7.5 and 10 µm), since the amount of minima is lower than for 2 µm within the same evaluation length.

The samples with 0° and 15° inclinations are characterized by a negative profile skewness and a platykurtic profile (< 3). A negative R_{sk} indicates a surface with plateau-like features, which is generally associated with a higher load-bearing capacity. Furthermore, the presence of deeper valleys may provide an important functional advantage by acting as reservoirs for wear debris, which can prevent third-body abrasion and stabilize the frictional behavior over the component's operational life. Furthermore, samples exhibiting less prominent inclinations also present a larger depth. Consequently, prior to an examination of the tribological performance, it could be hypothesized that the asymmetry should be enhanced, given that the shallower flanks might facilitate the counter body's glide. In contrast, when movement occurs in the UP direction, the larger structural depth creates a stronger barrier to the motion (e.g., a higher 'wall'), thereby enhancing the aforementioned interlocking mechanism. In contrast, the 30 and 45° inclined samples exhibit a positive skewness, suggesting a topography dominated by sharp peaks and deep valleys. This type of profile is expected to have a lower load-bearing capacity, as contact stress would be concentrated on the pronounced asperity tips. The 30° sample, in particular, shows a leptokurtic value (> 3), which implies a profile with numerous elevated peaks and troughs. Such a sharp topography could be more susceptible to asperity fracture and adhesive wear mechanisms under load.

3.2 Wear track analysis

Figure 4a–f shows representative wear tracks for all the configurations studied. All samples exhibit very similar wear tracks of approximately 70–80 µm in width. The main difference is observed in the wear mechanisms (see also Figure S2 in the supplementary material). The 0°, 30°, and 45°

Table 2 Topography descriptive parameters obtained from line profiles of the samples

Structural period /µm	Structural inclination /°	Descriptive parameters			
		R_c /µm	R_{sk}	R_{ku}	S-ratio
2	0	1.57 ± 0.04	− 0.46 ± 0.07	1.78 ± 0.10	2.568
	15	1.67 ± 0.06	− 0.46 ± 0.05	1.84 ± 0.03	2.625
	30	0.63 ± 0.04	0.21 ± 0.19	3.13 ± 0.23	1.586
	45	0.67 ± 0.03	0.24 ± 0.11	2.29 ± 0.18	1.782
7.5	15	2.01 ± 0.03	− 0.25 ± 0.01	1.63 ± 0.03	1.359
10	15	1.29 ± 0.03	− 0.27 ± 0.05	1.66 ± 0.04	1.301

The evaluation (sampling) length is 86.3 µm samples present some evidence of adhesive wear (identified by some material removal marks within the wear tracks), whereas in the 15° sample, the dominant wear mechanism appears to be plowing (plastic deformation). This is evidence of mild wear, resulting from a higher load-bearing capacity of the structures. On the other hand, adhesion is usually associated with higher mechanical stress, resulting in more severe wear. Further evidence of adhesion can be observed on the contact region of the counterbodies, which present evidence of material transfer (Figure S3). It is worth mentioning that in all cases, the original structured topography is recognizable in certain regions, indicating that it is highly likely that the grooves acted as a worn material reservoir, as previously reported for similar systems [14]. This is very important since it plays a fundamental role in the operational life of the components.

The trainable WEKA segmentation plugin tool in ImageJ (Fiji) was used to differentiate the wear track itself (red highlight) from debris-containing areas (purple highlight) and unmodified areas (green highlight) in the SEM micrographs, as shown in Fig. 4a. The training process was described in detail in [15]. The segmented micrographs from Fig. 4a were used to determine the average worn area and debris-containing area for each structured surface, presented in Fig. 4g. Considering the samples that were produced with the same inclination angle of 15°, the periodicity of the structures significantly changes how the surfaces are worn. The plot shows that as the periodicity of the structures produced increases from 2 to 10 µm, the average worn area decreases from approximately 5×10^3 µm^2 to 3.5×10^3 µm^2, respectively. Nevertheless, increasing the periodicity of the structures leads to an increase in the debris-containing area. This increment in debris-containing area with increased periodicity can be attributed to the fact that larger periodicities produce surfaces with skewness profiles that approach the mean plane—see Table 2. In other words, smaller periodicities produce surfaces with more material above the mean plane, potentially leading to more valleys that can capture wear debris, thus reducing the debris-containing area.

When considering the surfaces produced with the same periodicity of 2 µm and varying the inclination angle used to produce the asymmetrical structures, a clear relationship between worn area and debris-containing area can be observed (Fig. 4g). As the inclination angle increases, so does the debris-containing area, accompanied by a reduction in the average worn area. This reciprocal relationship between the worn area and debris-containing area suggests that higher debris retention within the wear track may lead to more severe wear, likely caused by three-body abrasion. The larger debris-containing area in the samples produced at higher inclination angles is caused by the relatively poorer debris-retention capabilities of these structures on account of their smaller structural depth. Moreover, as summarized in Table 2, for the same periodicity, higher inclination angles lead to a more positive skew (R_{sk}). This indicates that as the inclination angle increases, the height distribution of the material is shifted below the mean plane. This, in combination with the lower structural depth, enables structures produced at gentler angles to have more debris-retention capabilities. Vice versa, steeper production angles generate surfaces with poorer debris-retention capabilities. In this case, the debris is expelled from the wear track, thus leading to a higher debris-containing area and consequently reducing the likelihood of three-body abrasion. Compared to the reference sample (i.e., the symmetrical structures generated at 0°), structures produced at angles below 45° result in a lower debris-containing area. Nevertheless, as per the inverse relationship described, the worn area tends to be higher than the reference sample, particularly for the 15° sample. A possible compromise between wear and debris retention can be observed for the 30° sample. However, it should be noted that this sample exhibits the largest scattering among the configurations herein evaluated.

3.3 *Friction Asymmetry Characteristics for Fixed Period ($\Lambda = 2$ µm)*

Concerning the spatial evolution of the COF in both testing directions, typical curves for all the tested inclinations at a fixed structural period of 2 µm are shown in Fig. 5a–d. It is evident that in the 0° sample (i.e., symmetrical line structures) shown in Fig. 5a, both sliding directions show a smooth development, with very similar COF values irrespective of slide direction. The slightly higher COF in the DOWN direction is associated with a slight increase in the real contact area, which is a consequence of the successive removal of the structural features.

In the case of the asymmetrical structures shown in Fig. 5b–d, a distinct COF pattern is observed depending on the slide direction of the counterbody. As is the case in the symmetrical reference surface, the spatial COF evolution in the UP direction is relatively smooth and stable throughout the tribological tests. In the DOWN direction, on the other hand, a clearly jagged development is observed. The evolution of the COF resembles a saw-tooth profile, akin to the profile of asymmetrical structures. This behavior in the DOWN direction is related to the way in which the counterbody slides through the surface. Due to the asymmetrical structures, as the counterbody slides in the DOWN direction, the topography that the counterbody encounters varies significantly from low values at the top of the profile to high values when the ball contacts the steeper flanks. This behavior resembles that of a stick–slip system. In this analogy, the static coefficient of friction appears when the counterbody begins its ascend, followed by a sharp reduction in COF as it

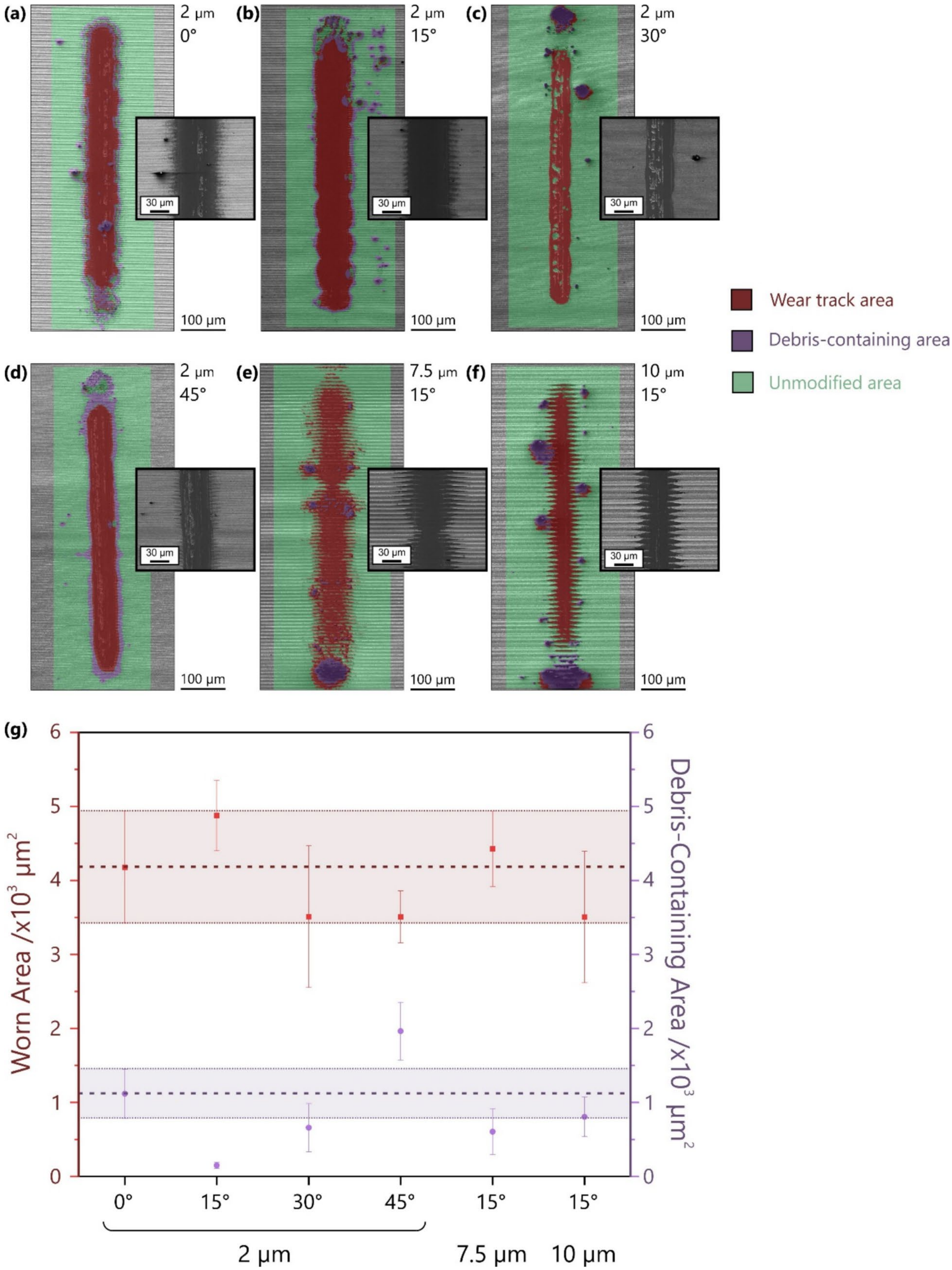
(a)
2 µm
0°
(b)
2 µm
15°
(c)
2 µm
30°
(d)
2 µm
45°
(e)
7.5 µm
15°
(f)
10 µm
15°
30 µm
100 µm
Wear track area
Debris-containing area
Unmodified area
(g)
Worn Area /x10³ µm²
Debris-Containing Area /x10³ µm²
0
1
2
3
4
5
6
0°
15°
30°
45°
15°
15°
2 µm
7.5 µm
10 µm

◂**Fig. 4** SEM images of representative wear tracks after 200 sliding cycles for **a** Cu-2 µm-0°, **b** Cu-2 µm-15°, **c** Cu-2 µm-30°, **d** Cu-2 µm-45°, **e** Cu-7.5 µm-15°, and **f** Cu-10 µm-15°. In each image, the upper right picture shows a detailed view of the center of the wear track. **g** The values of the segmented worn area and debris-containing area for each tested configuration. The shaded areas in the graph highlight the range for the symmetrical DLIP sample

overcomes the summit of the structures and the counterbody contacts the valley of the subsequent structure.

It is worth noting that within the inclined structures, there is also different variability in the COF values for the DOWN direction, ranging between 0.15 and 0.45, 0.18 and 0.45, and 0.20 and 0.45 for 15°, 30°, and 45°, respectively. Among the asymmetrical structures, the structures produced with an inclination angle of 30° stand out. The spatial evolution of COF in the DOWN direction, in particular, outlines the profile of the structures quite accurately. The structures produced at 15° and 45°, on the other hand, exhibit variability which does not describe the profile of the structures as well. Nevertheless, the asymmetrical behavior is still present after the 200 cycles.

Figure 5e–h shows the temporal evolution of the mean COF for each sample type throughout the 200 sliding cycles. A clear trend can be identified where for increasing inclination angles, the friction asymmetry effect starts to diminish. This is related to the fact that for lower inclinations, the DOWN faces tend to show milder slopes, whereas the UP faces tend to be steeper [1]. This naturally favors the motion in one direction (where the tangent of the inclination angle is lower) and enhances the interlocking effect in the opposite direction (the tangent of the inclination angle is larger).

Figure 5e presents a run-in development of a *type b* Blau curve [16], which is associated with a high initial wear rate until most asperities are removed. In typical rough technical surfaces, this contact situation would predominantly result in a *type c* curve. This type of curve is characterized by an increase in the COF until it reaches its initial peak, followed by a significant drop in COF and a gradual, mild increase in its value toward its steady state. This increase in the COF after its reduction is a result of the formation of wear debris, typically of wear in oxidized metals. However, this behavior is not observed in the reference sample (i.e., symmetrical structures) since the topographic minima allow the storage of wear debris. This debris-retention capacity stabilizes the COF's development, thus rendering a constant value once a stable contact area is established, thus leading to the *type b* curve. This debris-retention capacity of the structured surfaces is also observed in the asymmetrical structures. However, in this case, the COF curves resemble more a *type a* curve instead of a *type b*, particularly when sliding in the DOWN direction. *Type a* curves are characterized by a low initial COF value, followed by a gradual increase in COF that rapidly reaches its steady-state value. The increment in COF is typically due to the removal of superficial contaminants and oxide films, thereby leading to greater degrees of adhesion between the contacting surfaces.

All asymmetrical structures show a comparable run-in behavior, reaching steady state after 25–30 sliding cycles, whereas the reference sample requires closer to 50 sliding cycles to reach its steady state. Focusing on the temporal evolution of COF in the UP sliding direction, the COF values at the beginning and end of their run-in stages are similar,

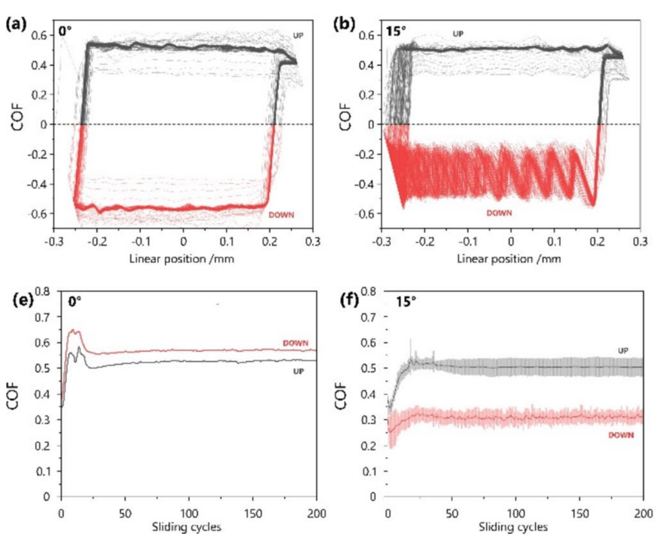

Fig. 5 Typical COF curves as a function of the position of the counterbody for 200 sliding cycles of **a** Cu-2 µm-0°, **b** Cu-2 µm-15°, **c** Cu-2 µm-30°, and **d** Cu-2 µm-45°. Mean COF curves of 3 tests as a function of the sliding cycles of **e** Cu-2 µm-0°, **f** Cu-2 µm-15°, **g** Cu-2 µm-30°, and **h** Cu-2 µm-45°

Table 3 Mean COF values for the different sliding directions and the asymmetry coefficient (ζ) for samples with different structural inclination (α) and fixed periodicity (Λ) of 2 µm

α	COF_{UP}	COF_{DOWN}	ΔCOF	ζ
0°	0.53	0.58	− 0.05	0.92
15°	0.50	0.31	0.19	1.65
30°	0.53	0.41	0.12	1.30
45°	0.54	0.46	0.08	1.17

irrespective of the production configuration. The initial COF value recorded is around 0.35, and its steady-state value is approximately 0.5. Nevertheless, as previously mentioned, the reference sample exhibits a *type b* COF curve, characterized by a larger COF peak during run-in, which in this case reaches a maximum value of approximately 0.55 (when sliding in the UP direction). Since the asymmetrical structures do not exhibit this peak, their run-in behavior culminates at or near the steady-state COF value of 0.5. This behavior of the asymmetrical structures could be associated with a steady and slow removal of the topographic maxima toward a constant contact area. However, it is worth mentioning that all studied configurations seem to be unaffected by the generated wear debris.

To quantify the asymmetry effect, an evaluation parameter ζ is defined as the ratio COF_{UP}/COF_{DOWN}, where values above 1 are desired for a smooth forward (DOWN) sliding process and an interlocking effect in the opposite direction (UP). Its values are summarized in Table 3.

The conventional DLIP sample (0°) showed an asymmetry value below 1. This can be traced back to a swift removal of the structures by contact in the very early stages of the tests (as discussed for the run-in behavior). Once the outstanding asperities are removed, a larger contact area is established, resulting in higher COF values. This is based on the Bowden–Tabor model [17], which establishes that the friction force arises from two interdependent forces (adhesion and deformation forces) and is directly proportional to the real contact area. Moreover, due to the symmetrical nature of these structures, negligible direction-dependent interlocking is observed. To further evaluate the robustness of the frictional asymmetry, an additional analysis based on the absolute difference $\Delta COF = COF_{UP} - COF_{DOWN}$ was performed. The obtained ΔCOF values show trends fully consistent with the ratio-based anisotropy coefficient ζ. In particular, the highest directional contrast in friction is observed for $\alpha = 15°$, whereas near-isotropic conditions correspond to small ΔCOF values and ζ close to 1. These results indicate that both parameters capture the same underlying physical mechanisms governing directional friction. Therefore, ζ is retained as the primary descriptor in this work, as it directly reflects the relative friction contrast, which is of primary relevance for applications such as directional motion control and bioinspired surface design.

From these values, it is clear that all inclined configurations exceeded the threshold value, where the 15°, 30°, and 45° inclinations present a + 65%, + 30%, and + 17% friction asymmetry, respectively. As previously mentioned, the difference within the configurations is given by the steepness of the DOWN flank, where the 15° configuration presents the mildest DOWN-face slope among the studied structures, hence exerting a lower mechanical interlocking resistance in this direction. This could be easily compared to a 'mechanical ratchet' mechanism that favors the interlocking of a pawl into a gear wheel in the UP direction. A further potential justification for the increased asymmetry coefficient of the 15° sample is the structural depth that results from this production configuration. Since the 30 and 45° samples exhibit much shallower structures with steeper DOWN faces, the COF when sliding in the DOWN direction tends to be more similar to the COF when sliding in the UP direction (as shown in Fig. 5f–h).

A direct correlation could be made between the topography and the observed tribological performance. The sample with a 15° inclination, which showed the largest friction asymmetry, is characterized by a negative skewness and a platykurtic, or evenly distributed, height profile (Table 2). This specific sample type, with a larger volume of material near the top of the profile, provides a better load-bearing capacity. Consequently, the dominant wear mechanism observed was plowing, rather than adhesion. Furthermore, the negative skewness indicates debris storage capability, which would help to stabilize the COF (as observed in the low standard deviation of both curves in Fig. 5f) by trapping wear particles within the topographic minima. On the other hand, the samples with 30 and 45° inclinations showed positive skewness values, indicating a profile with deeper valleys and sharper peaks. This topography likely resulted in a lower initial load-bearing capacity, leading to higher mechanical stress at the asperity tips. This is consistent with the observation of adhesive wear, which is typically associated with more severe contact conditions. The jagged COF development in these samples, particularly in the DOWN direction, can be attributed to the repeated interaction of the counterbody with these sharper, more defined asperities.

Based on the quantitative asymmetry coefficient (ζ), it is evident that a clear trend exists between the structural inclination and the resulting frictional anisotropy. The 15° inclination yields the most effective asymmetry. This confirms that the milder slope of its DOWN flank minimizes mechanical interlocking, while the steep UP flank maximizes it, resulting in the expected "*mechanical ratchet*" effect. As the inclination increases to 30 and 45°, the asymmetry diminishes; this reduction is attributed to the increasing steepness of the DOWN flank, which increases the frictional resistance in that direction and hence reduces the total difference between the two sliding directions. This consequently leads to an asymmetry coefficient that is closer to 1. Therefore, deep structures with mild structure slopes, as obtained in the 15° samples, are desired to maximize frictional asymmetry. This combination enables the minimization of three-body abrasion due to the debris-retention capacity of the deep structures, in addition to minimizing friction in the DOWN direction due to the low slope of the DOWN faces while also maximizing friction in the UP direction as the counterbody encounters the steep UP faces.

In contrast, the conventional DLIP sample (0°) serves as a benchmark, presenting an inverted asymmetry ($\zeta = 0.92$) compared to the inclined samples. This behavior could be associated with the initial wearing-off of the asperities, leading to an increased real contact area and, consequently, a higher friction force (as described by the Bowden–Tabor model). The fact that all inclined structures exceeded the $\zeta = 1$ threshold highlights the viability of the saw-tooth geometry in generating directional friction to different degrees. As a consequence of its better tribological performance, the 15° inclination was selected as the optimal configuration to further investigate the influence of varying the structural periodicity on friction asymmetry.

3.4 *Friction Asymmetry Characteristics for Fixed Inclination (a = 15°)*

Since the asymmetrical structures produced at 15° resulted in the highest degree of frictional asymmetry, it is interesting to evaluate the influence of structural periodicity on the directionally dependent friction behavior. Accordingly, the comparison now focuses on the 15° inclination, with structural periodicities of 2, 7.5, and 10 µm. The spatial and temporal evolution of the COF is shown in Fig. 6a–f**.**

The positional development of the COF (Fig. 6a–c) shows again a marked difference between the UP and DOWN directions for the different periodicities. The increase in the structural period seems to generate a slight offset in the linear position values, probably due to the fact that larger periods have wider regions where the contact is happening on the same topographical maxima. A quick estimation suggests that, under specific conditions, the contact region of the 2 µm system would contact a larger number of outstanding asperities (topographical maxima) at a given moment in time, assuming the counterbody slides under the same contact configuration for all systems. These estimations indicate that the number of outstanding asperities in contact at any given time could be 5 × or 3.75 × higher in the 2 µm system than in the 10 and 7.5 µm systems, respectively.

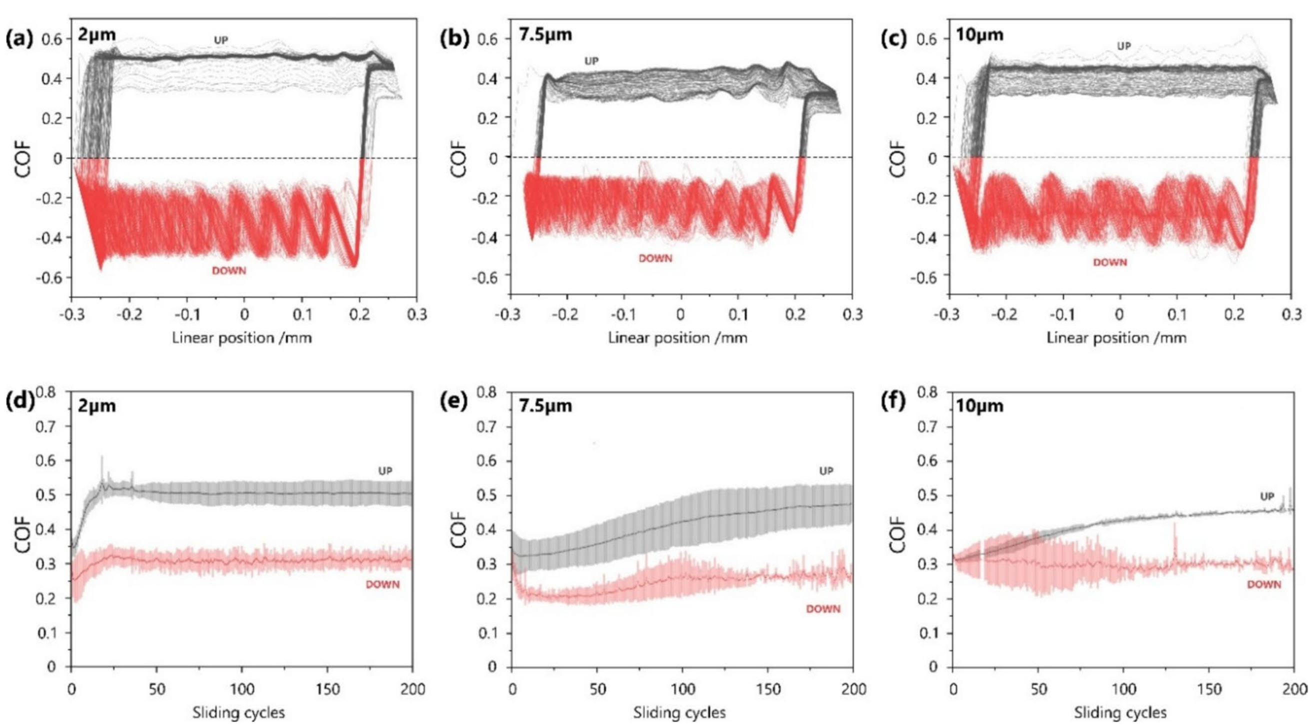

Fig. 6 Typical COF curves as a function of the position of the counter body for 200 sliding cycles of **a** Cu-2 µm-15°, **b** Cu-7.5 µm-15°, and **c** Cu-10 µm-15°. Mean COF curves of 3 tests as a function of the sliding cycles of **d** Cu-2 µm-15°, **e** Cu-7.5 µm-15°, and **f** Cu-10 µm-15°

Table 4 Mean COF values for the different sliding directions and the asymmetry coefficient (ζ) for samples with different structural periodicity (Λ) and fixed inclination (α) of 15°

Λ	COF_{UP}	COF_{DOWN}	ΔCOF	ζ
2 µm	0.50	0.31	0.19	1.65
7.5 µm	0.46	0.26	0.20	1.77
10 µm	0.45	0.30	0.15	1.5

All samples structured at an inclination angle of 15° exhibit similar structural depths (refer to Table 2), ranging between 1.3 and 2 µm, irrespective of structural periodicity. Nevertheless, recalling the worn area and debris-containing area analysis from Fig. 4, the wear track after the 200 sliding cycles is distinctly different, with a direct correlation between increased periodicity leading to smaller worn areas and lower debris-retention capacity. This is also reflected in the spatial COF evolution (Fig. 6a–c). These figures highlight the higher COF values in the 2 µm structures when sliding in the DOWN direction (between 0.1 and 0.5) compared to the 7.5 and 10 µm (between 0.1 and 0.4). The slightly lower COF observed in the 7.5 and 10 µm samples is likely due to the ejection of debris particles (on account of the reduced debris-retention capacity of these surfaces), which in turn reduces the likelihood of three-body abrasion.

As opposed to the 2 µm sample, the 7.5 and 10 µm surfaces do not seem to have reached the frictional steady state (Fig. 6d–f), likely due to a lower load-bearing capacity of the structures (as discussed in the interpretation of the surface descriptive parameters in Table 2). This results in a delayed establishment of a stable contact area throughout the tested cycles. Nevertheless, this might change once tribo-chemical and microstructural processes start to play a larger role in the interfacial contact.

On account of the stronger difference in the COF recorder when sliding in the UP and DOWN directions, the asymmetry coefficient for the structures produced at 15° and different periodicities is consistently above 1.5 (as shown in Table 4). This observation is further confirmed by the consideration of the ΔCOF values, which depict the same trend. This indicates a strong frictional asymmetry, therefore exhibiting the desired interlocking mechanism when sliding in the UP direction and a stick–slip-like behavior when sliding in the DOWN direction. This strong friction asymmetry of the structures produced at 15° can be explained by two key characteristics: i) all surfaces produced at 15° possess high structural depths, ranging from 1.3 to 2 µm; ii) the DOWN flanks have the most gradual slope, thus promoting lower COF in the DOWN direction. Therefore, from the asymmetry coefficient, it is clear that the optimal production inclination angle is 15°, with structural periodicity playing a less pivotal role in regard to the desired frictional asymmetry.

4 Conclusions

This study demonstrates the successful fabrication of bioinspired, asymmetrical topographies on laser-structured copper surfaces. By producing controlled saw-tooth structures, we established a straightforward and repeatable method for engineering surface friction anisotropy.

The main findings from this work are as follows:

- The laser-structured surfaces achieved a friction asymmetry of up to 77%. The degree of asymmetry, quantified by the asymmetry coefficient, is highly dependent on the manufacturing inclination angle. Shallower DOWN-face slopes (e.g., 7.5 µm/15°) maximize the directional friction effect.
- Shallower inclination angles produced deeper structural depths, which enhanced the surface's debris-retention capacity and reduced the likelihood of three-body abrasion.
- Despite the topographical modifications, all asymmetrical structures exhibited mild wear mechanisms (adhesion and plastic deformation) with worn areas comparable to symmetrical reference structures.

The ability to deterministically control friction asymmetry via DLIP offers significant potential for advanced tribological systems. These engineered surfaces provide a direct pathway for optimizing devices requiring directional friction, such as separable electrical contacts (where low insertion forces but high retention forces are desired) or soft robotics utilizing passive gripping.

While this work serves as a successful proof-of-concept, future studies will evaluate the long-term operational durability of these topographies beyond 200 sliding cycles, as well as their tribological performance under lubricated conditions and different atmospheres. Additionally, in the context of electrical contacts, the electrical contact resistance performance will also be evaluated.

Supplementary Information The online version contains supplementary material available at https://doi.org/10.1007/s11249-026-02136-x.

Acknowledgements This work made use of the resources of the Correlative Microscopy and Tomography (CoMiTo) core facility at Saarland University. Funding for PFIB/SEM by the German Research Foundation, grant number 415217285, is gratefully acknowledged. Furthermore, we would like to thank Dr. U. Pranav Nayak for their invaluable support with the WEKA segmentation analysis of the data used in this study.

Author Contributions Conceptualization: Sebastian Suarez and Fabian Bonner; Methodology: Fabian Bonner, Silas Schütz, and Sebastian Suarez; Software: Sebastian Suarez; Validation: Silas Schütz and Bruno Alderete; Formal Analysis: All authors; Investigation: Fabian Bonner; Resources: Frank Mücklich; Data Curation: Sebastian Suarez and Bruno Alderete; Writing-Original Draft Preparation: Sebastian Suarez; Writing-Review & Editing: Bruno Alderete, Fabian Bonner, Silas Schütz, and Frank Mücklich; Visualization: Sebastian Suarez; Supervision: Sebastian Suarez and Frank Mücklich; Project Administration: Sebastian Suarez; Funding Acquisition: Sebastian Suarez and Frank Mücklich.

Funding Open Access funding enabled and organized by Projekt DEAL. Funded by the Mat-Innovat project (grant number EFRE-HS-0000818), supported by the State of Saarland from the European Regional Development Fund (Europaischer Fonds fur Regionale Entwicklung, EFRE). In addition, this research was funded in part by the Deutsche Forschungsgemeinschaft (DFG, German Research Foundation) [Project number: SU911/2–1].

Data Availability The raw data supporting the findings of this study are publicly available under https://doi.org/10.5281/zenodo.17814735 at Zenodo.

Declarations

Conflict of interest The authors declare no competing interests.

References

1. Schütz, S., Suarez,S., Britz, D., Mucklich, F.: (2022) Generation of asymmetric topographic structures in Cu–Sn connectors using extended direct laser interference patterning for the tailoring of insertion and removal forces, in: Electr. Contacts, Proc. 67th Annu. Holm Conf. Electr. Contacts, IEEE, Tampa, US, p. 240. https://doi.org/10.1109/HLM54538.2022.9969800.
2. Tramsen, H.T., Gorb, S.N., Zhang, H., Manoonpong, P., Dai, Z., Heepe, L.: Inversion of friction anisotropy in a bioinspired asymmetrically structured surface. J. R. Soc. Interface. **15**, 20170629 (2018). https://doi.org/10.1098/rsif.2017.0629
3. Elbaum, R., Zaltzman, L., Burgert, I., Fratzl, P.: The role of wheat awns in the seed dispersal unit. Science **316**, 884–886 (2007). https://doi.org/10.1126/science.1140097
4. Rosenkranz, A., Reinert, L., Gachot, C., Mücklich, F.: Alignment and wear debris effects between laser-patterned steel surfaces under dry sliding conditions. Wear **318**, 49–61 (2014). https://doi.org/10.1016/j.wear.2014.06.016
5. Schütz, S., Suarez, S., Mücklich, F.: Tribo-electric analysis of multi-cycle wear in asymmetric laser-structured Cu-Sn connectors. Tribol. Lett. **71**, 1–12 (2023). https://doi.org/10.1007/s11249-023-01799-0
6. Arganda-Carreras, I., Kaynig, V., Rueden, C., Eliceiri, K.W., Schindelin, J., Cardona, A., Seung, H.S.: Trainable Weka segmentation: a machine learning tool for microscopy pixel classification. Bioinformatics **33**, 2424–2426 (2017). https://doi.org/10.1093/bioinformatics/btx180
7. Schäfer, C., Delfino, P.M., Leonhard-Trautmann, P., Ott, V., Suarez, S., Stüber, M., Mücklich, F., Pauly, C.: Fabrication of smooth , periodic surface structures: combining direct laser interference patterning and electropolishing. Adv. Eng. Mater. **27**, 2400435 (2025). https://doi.org/10.1002/adem.202400435
8. Lontin, K., Khan, M.: Interdependence of friction, wear, and noise: a review. Friction **9**, 1319–1345 (2021). https://doi.org/10.1007/s40544-021-0500-x
9. Crinon, E., Evans, J.T.: The effect of surface roughness , oxide film thickness and interfacial sliding on the electrical contact resistance of aluminium. Mater. Sci. Eng. A **242**, 121–128 (1998). https://doi.org/10.1016/S0921-5093(97)00508-X
10. Tamai, T.: Growth of oxide films on the surface of Cu contact and its effect on the contact resistance property. Electron. Commun. Japan **72**, 89–93 (1989). https://doi.org/10.1002/ecjb.4420720710
11. ISO 25178–2 Geometrical product specifications (GPS)—Surface texture: Areal—Part 2: Terms, definitions and surface texture parameters, (2021) 64
12. Zeng, Q., Qin, Y., Chang, W., Luo, X.: Correlating and evaluating the functionality-related properties with surface texture parameters and specific characteristics of machined components. Int. J. Mech. Sci. **149**, 62–72 (2018). https://doi.org/10.1016/j.ijmecsci.2018.09.044
13. Alamri, S., El-Khoury, M., Aguilar-Morales, A.I., Storm, S., Kunze, T., Lasagni, A.F.: Fabrication of inclined non-symmetrical periodic micro-structures using direct laser interference patterning. Sci. Rep. **9**, 1–12 (2019). https://doi.org/10.1038/s41598-019-41902-x
14. Reinert, L., Lasserre, F., Gachot, C., Grützmacher, P., MacLucas, T., Souza, N., Mücklich, F., Suarez, S.: Long-lasting solid lubrication by CNT-coated patterned surfaces. Sci. Rep. **7**, 42873 (2017). https://doi.org/10.1038/srep42873
15. Nayak, U.P., Müller, M., Britz, D., Guitar, M.A., Mücklich, F.: Image processing using open source tools and their implementation in the analysis of complex microstructures. Pract. Metallogr. **58**, 484 (2021). https://doi.org/10.1515/pm-2021-0039
16. Blau, P.J.: On the nature of running-in. Tribol. Int. **38**, 1007–1012 (2005). https://doi.org/10.1016/j.triboint.2005.07.020
17. Hutchings, I., Shipway, P.: Tribology - Friction and Wear of Engineering Materials. Butterworth-Heinemann, 2nd edn. Elsevier, Amsterdam (2017)